

Global Biogeochemical Cycles

RESEARCH ARTICLE

10.1029/2019GB006251

Key Points:

- We estimate methane (CH_4) emissions and sinks from wetlands and nonwetland soils for recent and future scenarios across the Contiguous United States (CONUS)
- Wetlands contribute most CH_4 emissions for the 2000s and increase in the future due to increasing temperature and wetland extent
- Nonwetland soils are a net CH_4 sink with emissions of CH_4 in some areas and sinks in other areas of the CONUS

Supporting Information:

- Supporting Information S1

Correspondence to:

A. K. Jain,
jain1@illinois.edu

Citation:

Shu, S., Jain, A., & Kheshgi, H. S. (2020). Investigating wetland and nonwetland soil methane emissions and sinks across the Contiguous United States using a land surface model. *Global Biogeochemical Cycles*, *34*, e2019GB006251. <https://doi.org/10.1029/2019GB006251>

Received 9 APR 2019

Accepted 25 MAY 2020

Accepted article online 7 JUL 2020

©2020. The Authors.

This is an open access article under the terms of the Creative Commons Attribution License, which permits use, distribution and reproduction in any medium, provided the original work is properly cited.

Investigating Wetland and Nonwetland Soil Methane Emissions and Sinks Across the Contiguous United States Using a Land Surface Model

Shijie Shu¹ , Atul K. Jain¹ , and Haroon S. Kheshgi² 

¹Department of Atmospheric Sciences, University of Illinois at Urbana-Champaign, Urbana, IL, USA, ²ExxonMobil Research and Engineering Company, Annandale, NJ, USA

Abstract We estimated the distribution of CH_4 emissions and sinks from wetlands (including freshwater and coastal wetlands) and nonwetland (including wet and dry soils) with a newly developed vertically resolved soil CH_4 model, integrated into a global land surface model (ISAM). We calibrated and tested this integrated model with CH_4 observations at test sites in the Contiguous United States (CONUS). ISAM is applied across the CONUS to estimate CH_4 emissions and sinks given both recent past observed climate and wetland extent, and future climate and wetland extent driven by two scenarios, RCP4.5 and RCP8.5. Estimated net CH_4 emissions for the 2000s are $13.8 \text{ TgCH}_4 \text{ yr}^{-1}$, mostly from wetland soils. Estimated net emissions under RCP4.5 and RCP8.5 are 30% and 64% higher, respectively, in the 2090s than in the 2000s due to (1) higher temperature and seasonal wetland extent (driven by higher precipitation in the climate scenarios), which increase modeled methanogenic activity more than methanotrophic activity in soils and (2) altered transport in the soil column and exchange with the atmosphere by modeled transport processes (diffusion, ebullition, and aerenchyma transport). Nonwetland soils emit CH_4 ($1.4 \text{ TgCH}_4 \text{ yr}^{-1}$) in some areas and take up CH_4 ($-2.9 \text{ TgCH}_4 \text{ yr}^{-1}$) in other areas, resulting in a net estimated sink for the 2000s; the net nonwetland soil sink increases by 15% and 46% by the 2090s under RCP4.5 and RCP8.5, respectively, mainly due to drier soil conditions, which enhances methanotrophic activity and oxidation of CH_4 diffused into soil from a future atmosphere with higher CH_4 concentration.

1. Introduction

Wetlands, including seasonal wetlands and wet soils, make up the largest natural source of methane (CH_4 ; Kirschke et al., 2013; Matthews & Fung, 1987), whereas dry soils are a CH_4 sink (Adamsen & King, 1993). The net exchange of CH_4 between these soils and atmosphere, as a consequence of methanogenic and methanotrophic activities in wetlands and soils, is highly variable in space and time (Topp & Pattey, 1997). The methanogenic process produces CH_4 under anaerobic conditions in wetlands and wet soils with a shallow water table depth (Angle et al., 2017). On the other hand, the methanotrophic process oxidizes CH_4 under aerobic conditions to form other compounds, such as formaldehyde, acts as a sink of CH_4 in dry soils. These processes are sensitive to soil conditions, including temperature, soil moisture, soil texture, soil pH, and water table depth (Cao et al., 1998).

Estimates for CH_4 emissions from wetlands at regional to global scales have received wide attention in the literature (Bloom et al., 2017; Potter et al., 2006; Saunio et al., 2016; Tian et al., 2010, 2012; Xu et al., 2010). Several studies have applied different methods to estimate the CH_4 emission and/or sinks for the Contiguous United States (CONUS). Potter et al. (2006) applied an empirical method that links the net ecosystem production (NEP) calculated from the CASA model to the CH_4 emission by multiplying a uniform CH_4 : CO_2 conversion factor, estimating CONUS emissions to be $5.5 \text{ TgCH}_4 \text{ yr}^{-1}$. Tian et al. (2010) developed a process-based global biogeochemical model, which coupled five core components (biophysics, plant physiology, soil biogeochemistry, dynamic vegetation, and land use management.), to estimate both CH_4 emissions and sinks from the soils, including wetlands. Xu et al. (2010) applied the same model to attribute the spatial and temporal variability of CONUS CH_4 emission to different environmental variables from 1979–2008 and found precipitation to be the most important factor. Tian et al. (2012) further synthesized the estimation of CH_4 emission and sink from multiple approaches for the whole North America and found a range of 3.3 – $9.1 \text{ TgCH}_4 \text{ yr}^{-1}$ for the CONUS region. The most recent global CH_4 budget study (Saunio et al., 2016)

estimated CONUS wetland emissions of 8–22 TgCH₄ yr⁻¹, based on top-down and bottom-up analyses. Wetlands, including seasonal wetlands, act as a major natural emission for the CONUS, contributing 25–45% of the total CH₄ emissions estimated by the bottom-up models (Saunio et al., 2016).

Precipitation events have been found to introduce variability in the magnitude of CH₄ sources and sinks from nonwetland soils (Ni & Groffman, 2018; Saunio et al., 2016), altering water table depth along with oxic and anoxic conditions on relatively short timescales. However, previous publications (Potter et al., 2006; Saunio et al., 2016; Tian et al., 2010; Xu et al., 2010), with the exception of Tian et al. (2012), did not provide estimates of both CH₄ emissions and sinks from nonwetlands across the CONUS. Also, these studies accounted for the effect of major environmental conditions on CH₄ emission (mainly focusing on the modeling of the CH₄ biogeochemistry dynamics), but these studies did not include a detailed linkage between soil hydrology and soil biogeochemistry, which is necessary for the more accurate estimation of both soil CH₄ emission and CH₄ sinks. While the importance of methanotrophic and methanogenic conditions and their interactions with soil conditions (e.g., temperature, soil moisture, soil texture, soil pH, and water table depth) were discussed in recently published landscape-level studies (Angle et al., 2017; Kaiser et al., 2018), the effects of these interactions on CH₄ emissions and sinks were not studied at a regional scale by the previously published studies mentioned above.

The overall objective of this study is to advance our understanding of the spatial and temporal distribution of CH₄ emissions and sinks from the wetlands, seasonal wetlands and nonwetlands (including wet and dry soils) for historical and future environmental conditions across the CONUS region using a land surface model, the Integrated Science Assessment Model (ISAM). Here wetlands refer to both inland freshwater wetlands and coastal wetlands. It is important to note that CH₄ emissions of coastal wetlands with high salinity are lower than inland wetland emissions due to relatively higher sulfate availability and generally higher abundances of sulfate-reducing bacteria, which outcompete methanogenesis (Poffenbarger et al., 2011). ISAM estimates CH₄ emissions and sinks from both wetlands and nonwetland soils under historical (1981–2015), as well as future environmental conditions under two future scenarios—RCP4.5 and RCP8.5—over the period 2016–2100 across the CONUS. In addition, the model also estimates soil CH₄ production, consumption, and three major transport processes (by aerenchyma, ebullition, and diffusion), which result in the spatial variation of CH₄ emissions and sinks. This study provides a foundation for understanding the spatial and temporal distribution of soil CH₄ sources and sinks for interpretation of atmospheric CH₄ measurements and budget, as well as the feedback between soil CH₄ emissions and climate change.

2. Model Description

To accomplish our overall objective, we first couple ISAM (El-Masri et al., 2015; Jain et al., 2005; Song et al., 2013; Yang et al., 2009) to a newly developed CH₄ module containing parameterizations of soil CH₄ dynamics. Each model grid cell is of 0.5° × 0.5° spatial resolution and is subdivided into 24 plant functional types (PFTs), including 20 vegetation types, desert, polar desert, bare soil, and land ice, based on the fractional area of PFTs (Meiyappan & Jain, 2012). The model is run at a 1-hr temporal resolution.

ISAM includes three coupled components: (1) a biogeophysical component, (2) a dynamic vegetation component, and (3) a soil biogeochemistry component. The biogeophysical component consists of soil energy, soil hydrology (Barman et al., 2014a, 2014b), and snow processes (Barman & Jain, 2016) and calculates energy and water fluxes (Barman & Jain, 2016; El-Masri et al., 2013). The hydrological model includes precipitation, dew formation, soil and canopy evaporation, canopy transpiration, surface, and subsurface runoff, groundwater discharge/recharge, and changes in water quantity (Barman et al., 2014b, Song et al., 2016). Soil water content is calculated based on Richard's equation and is redistributed with dynamic root growth and distribution in soil layers extended to a depth of 3.5 m globally, with the thickness of each soil layer increasing exponentially with the depth. The groundwater discharge/recharge process is implemented through a dynamic coupling between the bottom soil layers and an unconfined aquifer. The model accounts for the bedrock depth distribution based on the conterminous United States multilayer soil characteristics data set (CONUS-SOIL; Miller & White, 1998). The model calculates the thermal and hydrological properties for each soil layer as a function of soil liquid and ice water content, soil temperature, soil texture, and soil organic C and gravel content (Lawrence & Slater, 2008). To better estimate soil

hydrological properties in fine-textured soils, the model also considers the impacts of root growth, which changes the soil structure and properties, notably by affecting soil hydraulic conductivity in fine-textured soils (Song et al., 2016).

The dynamic vegetation component describes the above-ground C and N cycle through parameterization of the physiological processes, including photosynthesis, carbon, and nutrient allocation in the plant, plant phenology, and plant rooting depth for both natural vegetation (El-Masri et al., 2015; Yang et al., 2009) and cropland (Song et al., 2013, 2014).

In addition to CH₄ dynamics, a 10-layer soil biogeochemistry component was recently incorporated in ISAM to estimate the vertical soil organic C (SOC) and N (SON) profiles. This vertically resolved soil biogeochemistry component includes (1) vertical transport of SOC (including bioturbation and cryoturbation processes) and (2) vertically resolved SOC decomposition (Yang et al., 2009) and related environmental modifiers. The vertical transport of SOC among the soil layers is represented by diffusion-advection processes (Elzein & Balesdent, 1995). The environmental conditions are also linked to the SOC decomposition at each soil layer. The module is calibrated and evaluated against multiple observations of SOC and soil $\Delta^{14}\text{C}$ profile. The vertically resolved SOC module enables better representation of the SOC substrates for CH₄ production at different soil layers.

The maximum hydrologically active soil column depth used in ISAM was extended to 3.5 m (Barman et al., 2014a). The soil biogeochemistry component accounts for the processes governing the accumulation and formation of SOC and SON profiles include the vertical transport of SOC and SON, multilayer SOC decomposition, depth-dependent abiotic control on SOC decomposition and below-ground N processes (Yang et al., 2009). The model structure and parameters have been evaluated in previous literature (Barman et al., 2014a, 2014b; El-Masri et al., 2015; Gahlot et al., 2017; Jain et al., 2013; Meiyappan et al., 2015) and the performance of ISAM under multiple scales have been extensively evaluated in intercomparison projects (FACE-MDS: Walker et al., 2014; NACP: Schaefer et al., 2012; MsTMIP: Huntzinger et al., 2017; Mao et al., 2015; Zscheischler et al., 2014; GCP: Ahlström et al., 2015; Jung et al., 2017; Zhao et al., 2016).

2.1. Model Extension to Include CH₄ Dynamics

The CH₄ module (Figure 1) is coupled to ISAM through soil hydrology and soil biogeochemistry components to estimate soil CH₄ and O₂ sources and sinks, concentrations, and net emissions from the land to the atmosphere. In this study, we consider both inland freshwater wetlands and coastal wetlands. The CH₄ module shares the same 10 soil layers (to 3.5 m depth) as the soil biogeophysics and biogeochemistry modules, with the thickness of each soil layer increasing exponentially with depth (Barman et al., 2014a). Both O₂ and CH₄ transports in the soil column are represented in the model. O₂ has several orders of magnitude lower diffusivity in the water than in the air. Hence, soil saturation conditions below the water table tend to lead to anoxic zones, whereas drier conditions above the water table leading to oxic conditions. In anoxic conditions, organic matter is decomposed by methanogens that produce CH₄. Once CH₄ is produced in anoxic soils, it can diffuse to the atmosphere. On its way to the atmosphere, CH₄ can be partly or completely lost due to oxidation by methanotrophic bacteria in the soil oxic zone, which uses CH₄ as their only source of energy and carbon (Segers, 1998). CH₄ from the atmosphere can also diffuse into the nonwetland soil column (Equation S1.27 in the supporting information), and this diffused CH₄ can also be oxidized (See Text S1.4 for the detailed description). A detailed description of the module can be found in supporting information Text S1, and all the related equations are described in supporting information Table S2. All the abbreviations appearing in the paper main text and in the equations are described in Table S1. The CH₄ module developed here accounts for all the major processes affecting the aqueous and gaseous phase volumetric concentration of both CH₄ and O₂ in the soils.

The CH₄ module accounts for six specific processes: (1) soil CH₄ production in the soil column by methanogenic activities (P), (2) soil CH₄ released to the atmosphere by gas diffusion (FD_{\uparrow}), (3) transport of CH₄ from the root zone of aerenchymatous plants to the atmosphere (A), (4) ebullition from wetlands to the atmosphere (E), (5) soil CH₄ loss in the soil column by CH₄ oxidation in the soil (O), and (6) atmospheric CH₄ uptake by soil due to gas diffusion (FD_{\downarrow}). Here we report the net diffusion flux ($FD = FD_{\uparrow} - FD_{\downarrow}$) calculated using the Equation S1.28. A positive FD represents a CH₄ emission to the atmosphere.

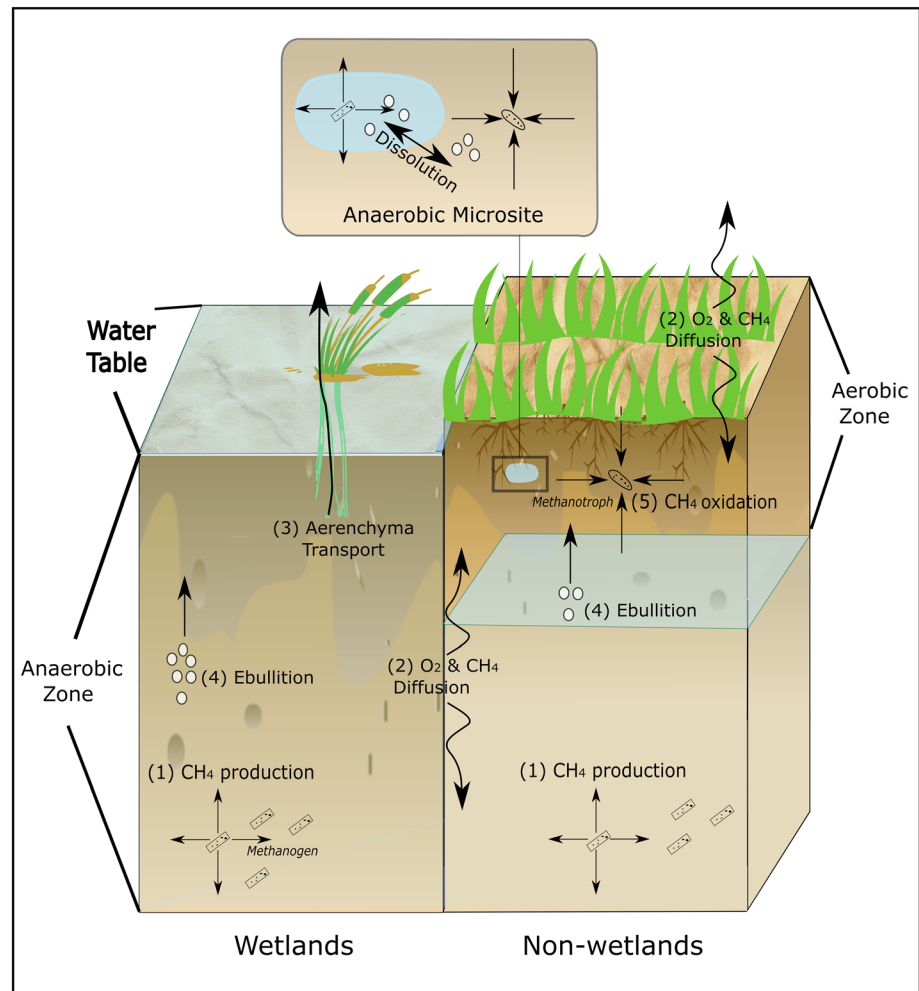


Figure 1. The schematic diagram illustrates the CH₄ dynamic processes represented in the ISAM CH₄ module. The module includes CH₄ production through methanogens in the anaerobic zone; CH₄ transport in the soil column and to the atmosphere through diffusion; CH₄ transport to the atmosphere through aerenchyma and ebullition; and CH₄ consumption through methanotrophs in the aerobic zone. The module treats wetlands and nonwetlands differently. For permanent wetlands or seasonal wetlands, the entire soil column is considered anaerobic, and ebullition is included as a direct pathway for CH₄ transport to the atmosphere. For nonwetlands, CH₄ oxidation in the aerobic zone consumes the CH₄ transported upward from the anaerobic zone below the water table, or CH₄ that may diffuse downward from the atmosphere insufficiently to dry soils. The model couples all these functions with the dynamics of soil biogeophysics (energy and hydrology) and biogeochemistry (carbon and nitrogen cycles), which enables the estimation of soil CH₄ sources and sinks under a variety of climate and soil conditions across the CONUS.

The soil production and losses of CH₄ are linked to the hydrological dynamics in the model. ISAM first calculates soil moisture with a hydrology module, and then the diffusion of the O₂ in the soil column to determine the O₂ concentration in soil. Production of CH₄ happens in anoxic soil where the soil is saturated, and O₂ concentration is low. Anoxic conditions also exist in unsaturated soil where anoxic microsites have limited access to O₂ due to the soil tortuosity (Angle et al., 2017). Losses of CH₄ are considered in the model through the CH₄ oxidation where O₂ concentration is high in dry soil layers.

Since ISAM soil hydrology dynamics are coupled with CH₄ production and oxidation, the variation of the water table calculated from ISAM affects the magnitude of CH₄ production and oxidation, and hence net CH₄ emission. Soil with a shallower water table contains more saturated soil for CH₄ production and less unsaturated soil for CH₄ oxidation and thus has a higher CH₄ emission than the soil with a deeper water table. This linkage in the model can result in changes in CH₄ emissions due to the variation of the water

table; for example, the deepening of the water table following a drought period can reduce the CH₄ emissions.

The aqueous and gaseous phase concentrations of CH₄ and O₂ for each soil layer are calculated using Equations S1.1a–S1.1d. The various phases of diffusion rates of CH₄ and O₂ at each soil layer (Equations S1.7–S1.11 and supporting information Text S1.1) are determined based on soil texture, the soil water table depth (z_{wt}), and soil moisture (Millington & Quirk, 1961; Moldrup et al., 2003) with boundary conditions given by Equation S1.12. The atmospheric CH₄ and O₂ concentrations are calculated using Equation S1.13. The sum of all sources, sinks and transportation fluxes of CH₄ and O₂ from soil to atmosphere (Equation S1.14), including P (Equations S1.15–S1.17), O (Equations S1.18–S1.20), E (Equations S1.21–S1.23), and A (Equations S1.24–S1.26) are added to the diffusion equation, Equation S1.1. The diffusion equation is then solved using the Crank-Nicholson finite differencing method. Finally, the sum of wetlands (N_w) and nonwetlands (N_{nw}) soil CH₄ emission $EM (= N_w + N_{nw})$ equals to the sum of FD , E , and A fluxes, where $FD (= FD_w + FD_{nw})$ is the sum of wetlands (FD_w) and nonwetlands (FD_{nw}), is described by Equations S1.28–S1.29.

ISAM accounts for wetland and nonwetland soil types within a grid cell (defined as a time-varying fraction of the grid cell), rather than assuming the entire grid cell to be either wetlands or nonwetlands. The wetland differs from the nonwetland in the calculation of soil hydrology and soil biogeochemistry. We have added SOC and SON pools for all wetland-specific biogeochemical processes in the soil biogeochemistry component. Aerenchyma development can happen for plants in seasonal anoxic soil and also in nonwetlands under seasonal wet soil with partial waterlogging conditions (Jackson & Armstrong, 1999). Therefore, ISAM includes aerenchyma transport not only for wetlands but also for nonwetlands. The model also accounts for the salt water intrusion for the coastal wetlands (hereafter referred to as coastal wetland effect), which reduces the methanogenesis. This effect is parameterized by calibrating the value of CH₄/CO₂ production ratio parameter ($r_{CH_4:CO_2}$). The effects of sea level rise on the future changes in coastal wetland extent are also considered using the parameterization scheme described in section 3.

Two types of wetlands (marsh and saltwater marsh) considered in ISAM are dominated by the herbaceous plants (more than 95%), a small amount of forest (i.e., mangrove, about 0.53%) (Krauss et al., 2011), and crop (i.e., rice, about 2.3%; Portmann et al., 2010) over the CONUS. In ISAM herbaceous wetland plants are C3 and C4 grasses, the mangrove forest is forest PFT (Krauss et al., 2011), and the crop is rice. We calibrated/evaluated the model for the herbaceous wetland plants using seven sites (see section 5.1). For rice, we applied a specific calibrated parameterization describing rice phenology (Lin et al., 2017) and use one rice site for model calibration. There is no other rice FLUXNET site in the CONUS that provides sufficient information to evaluate ISAM. In addition, there is no AMERIFLUX site for mangrove wetlands (Knox et al., 2019) in the CONUS. Therefore, we are not able to calibrate/evaluate ISAM for forest wetland type.

The coupled model was first calibrated and evaluated with site-level data, including CH₄ sources and sinks, which is described next.

3. Model Calibration and Evaluation

Measured CH₄ fluxes from 10 FLUXNET sites across the CONUS region were used to calibrate and evaluate model parameters (Table 2), including aerenchyma transport factor (F_{aere_s}), $r_{CH_4:CO_2}$, potential CH₄ oxidation rate (O_{PM}), Q_{10} coefficient and scaling factor of ebullition threshold (F_{ebul_s}), and evaluate ISAM-calculated CH₄ fluxes at each site. Based on the FLUXNET network, we found site data for three different types of wetlands (i.e., marsh, rice, and salt marsh) and upland. Marsh and rice are the freshwater wetlands and salt marsh is a saline water wetland. Overall, we used five sites (two sites for marsh and one site each for the salt marsh, upland, and rice) for model calibration, and five sites (three sites for marsh and one site each for salt marsh and upland) for model evaluation. To evaluate modeled emissions for upland, we used the results from Curry (2007) for the Colorado State measurement site and for the regional scale to show that ISAM results are consistent with the Curry (2007) in section 5.2. While there are emissions data available for additional sites (e.g., Knox et al., 2019; Olefeldt et al., 2013; Turetsky et al., 2014), missing input data for ISAM at these sites limits their use for evaluation. The data is also available for the peatland sites (e.g., Iversen et al., 2018), but we can not use these sites data, because the model does not account for

Table 1
Site Information of AMERIFLUX Sites Used for Model Calibration and Evaluation for the CONUS

Site (code)	Location (lat, long)	Function	Data period	Wetland type	Soil texture (%) (porosity/clay/sand)	MAP (mm)	MAT (°C)	Reference
Winous Point North Marsh (US-WPT)	41.465, -82.991	Calibration	2011–2013	Marsh	45.1/23.0/36.0	849	10.1	Chu et al. (2015)
Twitchell Island West Pond (US-Tw1)	38.109, -121.653	Calibration	2013–2015	Marsh	42.6/24.0/56.0	421	15.5	Oikawa et al. (2017)
Mayberry Wetland (US-Myb)	38.049, -121.765	Evaluation	2012–2015	Marsh	42.6/13.0/35.0	338	15.9	Matthes et al. (2014)
Disney Wilderness Preserve Wetland (US-DPW)	28.052, -81.436	Evaluation	2013–2015	Marsh	45.6/20.0/32.0	1,142	22.6	Knox et al. (2019)
Old Woman Creek (US-OWC)	41.379, -82.512	Evaluation	2015–2017	Marsh	46.6/16.0/36.0	930	10.7	Rey-Sanchez et al. (2018)
St Jones Reserve (US-StJ)	39.088, -75.437	Calibration	2018	Salt marsh	42.5/26.0/52.0	1,121	13.5	Knox et al. (2019)
Pointe-aux-Chenes Brackish Marsh (US-LA1)	29.501, -90.445	Evaluation	2011–2013	Salt marsh	62.2/36.0/26.0	1,625	20.7	Knox et al. (2019)
Howland Forest (US-Ho1)	45.204, -68.740	Calibration	2016–2017	Upland/forest	46.7/19.0/23.0	1,070	5.27	Knox et al. (2019)
Curtice Walter-Berger cropland (US-CRT)	41.628, -83.347	Evaluation	2011–2013	Upland/crop	45.1/24.0/56.0	849	10.1	Chu et al. (2014)
Twitchell Island (US-Twt)	38.109, -121.653	Calibration	2012–2013	Rice	42.6/24.0/56.0	421	15.6	Baldocchi et al. (2016)

peatland soil dynamics. We note that while the US-Tw1 marsh calibration site and US-Myb marsh evaluation site are located less than 15 km away from each other, their soil texture, porosity, and water table depths are different (Oikawa et al., 2017; Table 1).

Site-specific observation data for seven climate variables (surface air temperature, specific humidity, precipitation rate, surface wind speed, surface air pressure, incoming shortwave radiation, and incoming long-wave radiation) and water table depth were inputs into ISAM to drive ISAM's emission flux response. A brief description of each site is provided in Table 1.

Site-level ISAM simulations for calibration and evaluation were performed in two steps. First, the model was spun-up for each site with the original values of the five model parameters given in Table 2; these parameters

Table 2
The Equations for the Major Processes and the Corresponding Parameters Are Calibrated in This Study

Calibrated process equations		Parameter	
		Original value	Calibrated value
Aerenchyma transport	$A = F_{aere_s} (C^a - C_{eq}^a + (C^a - C_{eq}^a) e^{(\frac{y_{k_filler}}{\theta_w \Delta z})}) \theta_w \Delta z$	F_{aere_s}	1.0 0.75
CH ₄ production	$P = R_h \times r_{CH_4:CO_2} \times F_{te_m} \times F_{an_m}$	$r_{CH_4:CO_2}$	0.1 0.06 ^a , 0.03 ^b
Sink due to oxidation for CH ₄ and O ₂	$O = O_{PM} \frac{C_{O_2}^g}{k_{O_2} + C_{O_2}^g} \frac{C_{CH_4}^g}{k_{CH_4} + C_{CH_4}^g} \theta_a \Delta z$	O_{PM}	0.058 mmol m ⁻³ s ⁻¹ 0.06 mmol m ⁻³ s ⁻¹
Temperature modifier	$F_{te_m} = Q_{10}^{\frac{(T_s - 25)}{10}}$	Q_{10}	2.0 2.2
Maximum CH ₄ concentration in soil water	$C_{CH_4,max} = F_{ebul_s} V_{CH_4,max} \frac{P_a + \rho g(z - z_{wt})}{R_{gas}(T_s + 273.16)}$	F_{ebul_s}	0.25 0.65

Note. The original parameter values are without calibrated values. The calibrated parameter values are the mean value of the parameters for each of the three calibrated sites, US-WPT, US-Tw1, and US-STJ1. The description of all the variables is given in Table S1, and the descriptions of all the equations can be found in supporting information Text S1.

^aFor inland freshwater wetlands. ^bFor coastal wetlands.

were then calibrated in the second step. For this step, atmospheric CO₂ and CH₄ concentrations, and N deposition were set at 1981 levels. Since climate forcing and water table depth from site observations are only available for a limited number of years (Table 1), we recycled the site-specific climate data and water table depth until the SOC profile reached a steady state. Second, we calibrated five different model parameters (Table 2) by iteratively running the model over the period 1981–2010 using time-dependent observed atmospheric CO₂ and CH₄ concentrations, N deposition and climate forcing data, as well as by varying the parameter values until we found a set of parameter values that minimized the root-mean-square errors (RMSEs) between the simulated and the observed daily net CH₄ flux. We used the FORTRAN implementation of the Feasible Sequential Quadratic Programming (FFSQP; Zhou et al., 1997) numerical optimization scheme to adjust the parameter values in each iteration. In cases where the optimization scheme was not able to find a set of parameters with an RMSE less than 0.5 (e.g., in cases where observations have a high year-to-year variation), we manually adjust the parameters via the trial and error method to minimize the RMSE. Next, we evaluated the model for two independent sites using the average values of each calibrated parameter for sites. The site-level evaluation is done using the refined Willmott's index (Willmott et al., 2012) method described in supporting information Text S4.

4. CH₄ Emissions Across the CONUS: Input Data, Model Experiments, and Results

The coupled ISAM model was used to estimate CH₄ emissions over historical conditions (1981–2015), and future scenarios (2016–2100) across the CONUS region using the datasets described next.

4.1. Input Data

1. *Gridded climate forcing.* For the historical simulation over the period 1981–2015, we used CRUNCEP climate forcing reanalysis data for the same seven near-surface climate variables we used for model calibration described in the previous section (Harris et al., 2014). For the future simulations under scenarios RCP4.5 and RCP8.5 over the period 2016–2100, we used the CESM1BGC fully coupled model results for climate forcing data (Ren et al., 2018). The CESM1BGC future atmospheric variables have biases as compared to the CRUNCEP reanalysis, which we addressed by adjusting the mean and standard deviation of the future datasets (see details in Text S2).
2. *Atmospheric CO₂ and CH₄ concentrations and N depositions.* Historical inputs for atmospheric CO₂ and CH₄ concentrations were taken from Le Quéré et al. (2018) and Dlugokenky (2018), and N deposition from Lamarque et al. (2011). The projection of these variables for future scenarios RCP4.5 and RCP8.5 was obtained from the output of the CESM1-BGC coupled simulation (Ren et al., 2018).
3. *Gridded land cover (LC) or PFT data.* We applied LC data for the year 2000 that was reconstructed from the Historical Database of the Global Environment (HYDE 3.1) by Meiyappan and Jain (2012). LC data did not change with time in our analysis, as our study focused on natural terrestrial CH₄ emissions. We assumed that for the wetland fraction with permanent surface water coverage, the dominating LC would be marshes with strong anoxic conditions. In the model, we treated grasses as marshes, if they exist along with wetlands in a grid cell, since the presence of marsh prevents other dense root PFTs to survive. For grid cells with seasonal wetlands and/or the seasonal nonwetland fractions, any PFT along with seasonal wetlands and/or seasonal nonwetlands could exist in a grid cell.
4. *Gridded soil texture and topographic slope data.* We forced ISAM with the newly available global soil texture dataset GSDE (Shangguan et al., 2014), which was generated by merging various regional and national soil databases and soil maps. The topographic slope data used is from the U.S. TOPO Map (<http://nationalmap.gov/ustopo/index.html>).
5. *Gridded surface inundation data.* The fractional area of permanent wetlands and seasonal or inundated wetlands within each 0.5° × 0.5° model grid cell was prescribed using the Surface Water Microwave Product Series dataset (SWAMPS, Schroeder et al., 2015) for the period 1992–2012. This data determined the wetland extent within each model grid cell based on the fractional surface area of the grid saturated with water (*FW*; Figure 3a). The fraction of nonwetlands within each model grid cell was then determined by subtracting the *FW* from 1.00 (Figure 3b). To better account for the role of coastal wetlands in our estimation, we used the coastal wetland extent fraction data of Schuerch et al. (2018), which we combined with wetland extent data in each grid cell along the coastline.

Within a grid cell, both wetlands (including freshwater and coastal) and nonwetlands can coexist. Since the SWAMP data does not include open water, for example, river and lake, we did not calculate CH₄ emissions from these waters. Logistic functions fit to rainfall data extending from the most recent decade through the future scenarios were used to represent freshwater wetland area under the two future scenarios for 2016–2100. To project coastal wetland extent, we first calculated the wetland fraction using the same approach as for freshwater wetlands and then subtracted from this the fraction of the coastal wetlands lost due to the sea level rise provided by Schuerch et al. (2018). According to this data, the estimated loss of coastal wetlands due to sea level rise over the period 2010–2100 was 6% for the RCP4.5 and 19% for the RCP8.5. See Text S3 for details of this method.

4.2. Experimental Design of Model Results

ISAM was used to estimate the net CH₄ emissions (*EM*) equation (Equations S1.28a and S1.28b) over the CONUS for a historical period and two alternative future climate scenarios: RCP4.5 and RCP8.5. For regional simulation over the CONUS, we directly applied the fraction of each PFT based on the land use data (Meiyappan & Jain, 2012). For the mangrove forest we applied mangrove mask data of Giri et al. (2011), and for the rice crop we applied the rice mask data of Portmann et al. (2010).

Before the start of these two simulations, the model was first spun-up using a similar approach as used for site-level simulation: that is, forcing the model by repeating CRUNCEP climate forcing from 1981–2015 over 750 years with atmospheric CO₂ and CH₄ concentrations fixed at 1981 levels (337.7 ppm and 1,504.9 ppb respectively) and spatially resolved N deposition also fixed at 1981 levels.

Next, the model was run for the historical period 1981–2015 with the varying historical atmospheric CO₂, CH₄, N deposition, and climate forcing data discussed above. For the two future scenarios, RCP4.5 and RCP8.5, the model was forced over the period 2016–2100 with spatial and temporal varying climate forcing data, atmospheric CO₂ and CH₄ concentrations, and N deposition data (see section 4.1).

Model-estimated CH₄ emissions from wetlands and nonwetlands for the current and future environmental conditions over the CONUS are reported in section 5. Wetlands consist of permanent and seasonal wetlands (hereafter wetlands). Nonwetlands can be seasonal wet soil or seasonal dry soil (hereafter nonwetland soil). The spatial distribution of CH₄ emissions and sinks for each grid cell and the regional total values for the CONUS are reported for wetlands and nonwetlands (wet and dry soil emissions combined) averaged for the period 2001–2010 (hereafter referred to as 2000s) and the change for the averaged period 2091–2100 (hereafter referred to as 2090s) relative to the 2000s under two future scenarios, RCP4.5 and RCP8.5. Model results are also compared with other existing model results of historical wetland emissions.

To evaluate ISAM performance for the CONUS, ISAM-estimated wetland CH₄ emissions are compared with a recent product of the global wetland CH₄ emission model ensemble for use in atmospheric chemical transport models (WetCHARTs, Bloom et al., 2017), which we compiled for the period 2009–2010.

5. Results and Discussion

5.1. Model Calibration and Evaluation

Model calibration and evaluation results for *EM* for five calibrated sites (Figures 2a, 2c, 2f, 2h, and 2j), and for five evaluated sites (Figures 2b, 2d, 2e, 2g, and 2i) show a large variations in estimated seasonal and annual *EM* across all sites, because these sites are diverse (i.e., eight wetland sites and two upland sites) but with different PFT distribution. Therefore, CH₄ production, ebullition, and aerenchyma transport are also diverse across all sites. This is also reflected by the relatively large variations in calibrated parameter value for F_{aere_s} , $r_{\text{CH}_4:\text{CO}_2}$, and F_{ebul_s} across five calibrated sites, suggesting that the processes and soil inputs (e.g., soil texture), which these parameters relate to, are diverse across calibrated sites.

Nevertheless, ISAM results are able to capture the overall observation of the seasonal variations of *EM* at calibrated and evaluated sites. The agreement between model results and observations for most of the sites, with the exception of one salt marsh site (US-StJ) and both upland sites, is also supported by higher (lower) refined Willmott's index and R^2 values (Table 3). The sites with high Willmott's index and R^2 have a good fit for both the absolute values and seasonal variations between model simulations and observations, while sites with low mean error (ME) show a good fit of absolute values.

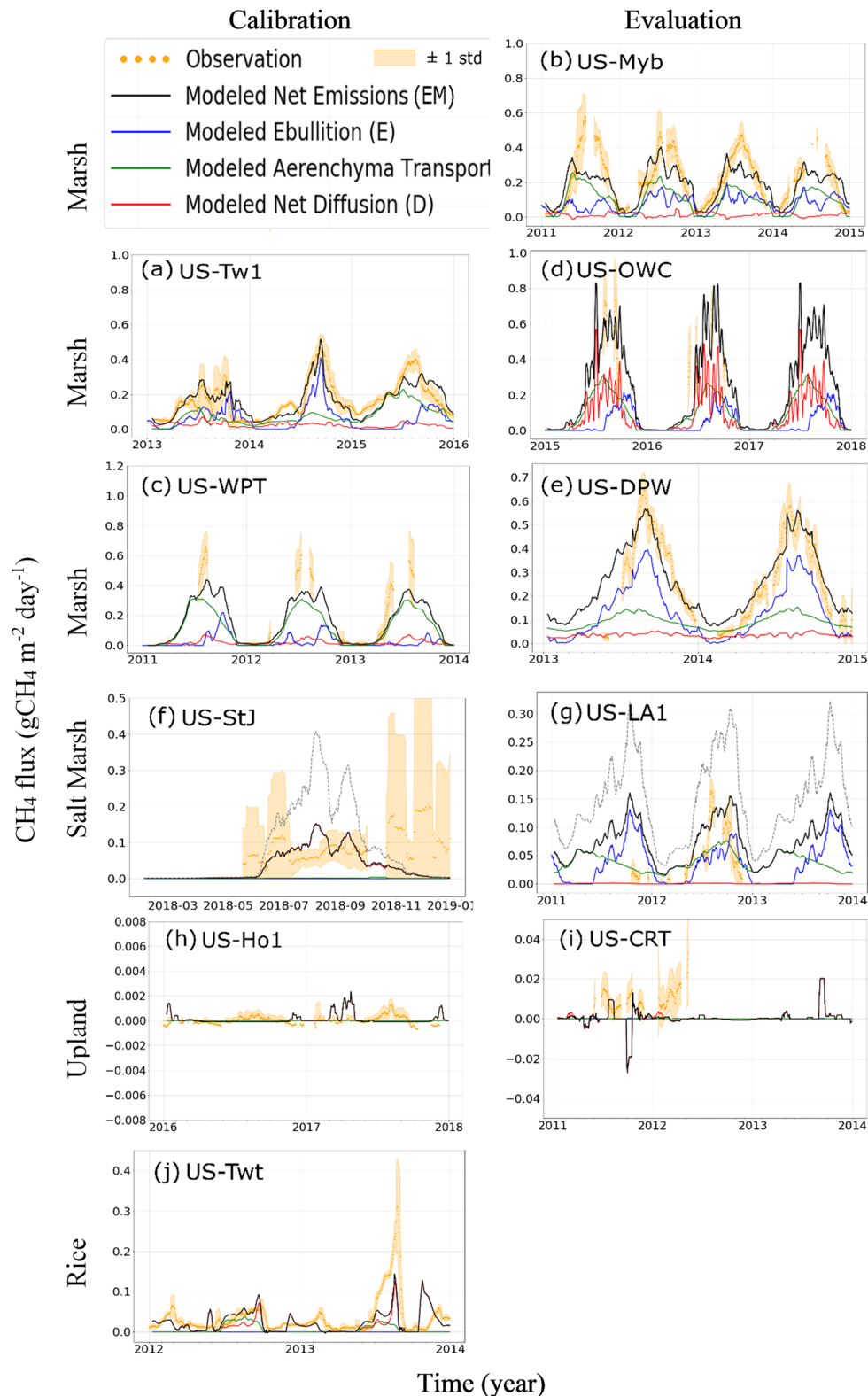


Figure 2. Comparison between ISAM modeled and observed 20-day moving-average daily net CH_4 fluxes from the soils for five calibrated sites (a, c, f, h, and j) and five evaluated sites (b, d, e, g, and i). The main characteristics of these sites are provided in Table 1. The model calibration and evaluation are performed over the time periods of the available observation data, which varies from site to site. The solid yellow dots show the available observations and the yellow shaded areas show the one-standard-deviation range of daily observations within each 20-day moving average. The dash gray lines in (f) and (g) show ISAM simulation results without including the reduction factor of salinity for CH_4 production.

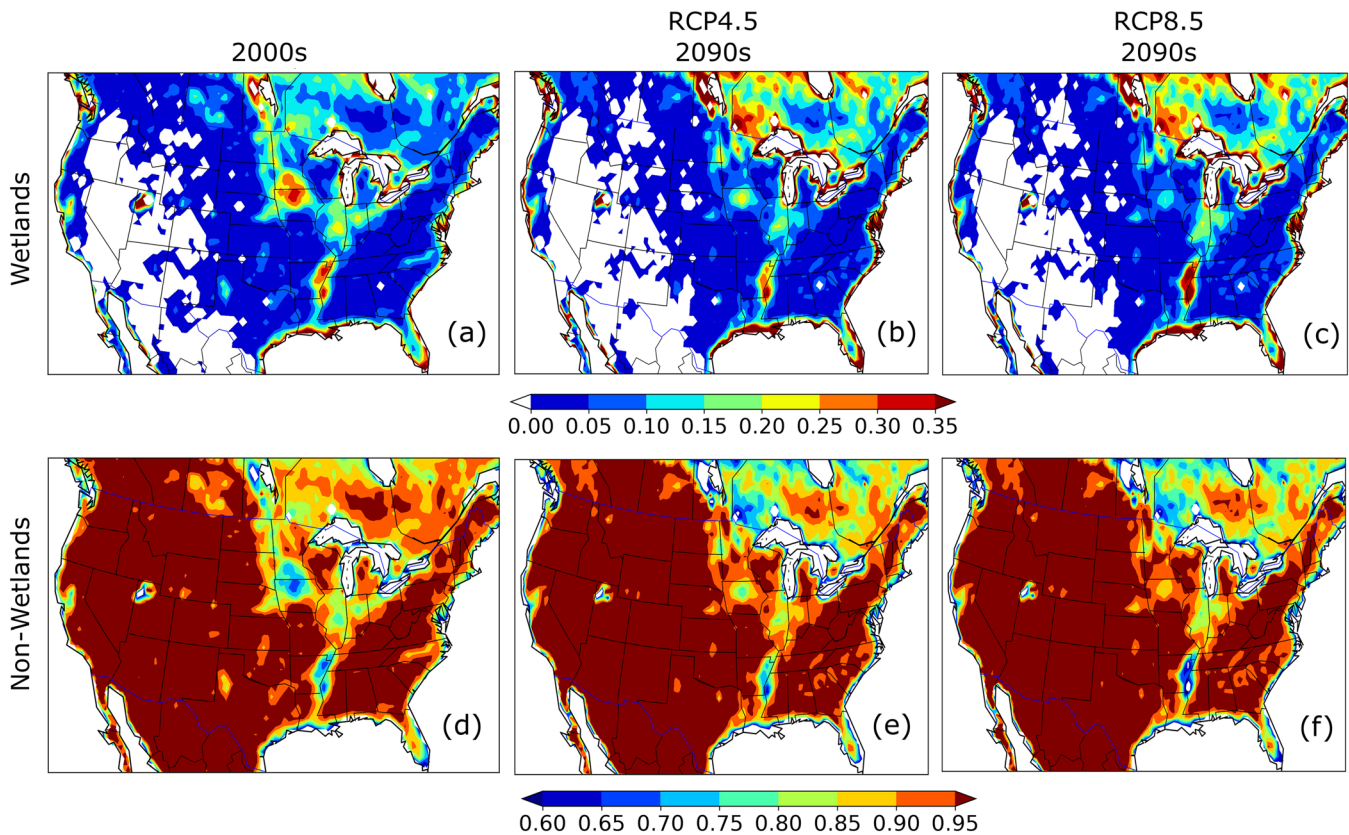


Figure 3. The fraction of permanent and seasonal wetland extent is shown by panels (a)–(c), and the fraction of nonwetland extent is shown by panels (d)–(f). The values are averaged over the 2000s (a, d), and the 2090s under the RCP4.5 scenario (b, e), and the 2090s under the RCP8.5 scenario (c, f). The color bars for Rows 1 and 2 represent the fraction of wetlands and nonwetlands (ranging from 0 to 1) of each grid cell averaged over each time period.

While the model estimated *EM* magnitudes for most of the sites compared reasonably well with observation data, model is not able to capture peak *EM* for few sites. For example, model is not able to capture the peak of CH_4 emission within a year at the US-Myb site, suggesting the underestimation of the *EM* during the period with peak plant productivity (Knox et al., 2017). The plausible cause of such discrepancy is that model is missing site-level input data, including the soil texture and plant community. In addition, most of the available site-level datasets do not provide observation information for CH_4 production, oxidation, and three different transport pathways, which makes the model validation task challenging.

The CH_4 fluxes show high seasonal variation governed by the aerenchyma transport and ebullition, which contribute the most to the total CH_4 emissions for various marsh sites (Figures 2a–2e). However, it is important to note that marsh sites are showing two different types of seasonal behavior based on the modeled emissions fluxes. While the seasonal peak in Tw1 and DPW are dominated by ebullition, the seasonal peak in the other three marsh sites is dominated by aerenchymous transport. Although published literature on these sites do not report any information about the contribution of different transport pathways of the CH_4 *EM*, a general linkage between plants' root tissues and a relatively larger root volume supports a larger aerenchyma transport at the time of higher productivity (Bhullar et al., 2013), which is also supported by ISAM results for Myb, WPT, and OWC sites, suggesting that plant roots contain more biomass at these sites compared to Tw1 and DPW sites. Thus, yield estimations being dominated by aerenchyma transport at these sites. In contrast, ISAM results for Tw1 and DPW suggest the production of CH_4 causing a buildup of soil CH_4 bubbles during the days after peak production. As these trapped CH_4 bubbles grow in size over time, the level of the soils where CH_4 bubbles residing in also rises slowly as well, and eventually trigger the ebullition, resulting in the release of CH_4 bubbles to the atmosphere in late summer and early fall. This is the reason that the peak emissions for Tw1 and DPW sites occur not at the time of peak CH_4 production, but at a

Table 3

The Calculated Refined Willmott's Index, Goodness-of-Fit of Linear Regression (R^2), and the Mean Error (ME) for Net CH_4 Emission (EM), on a Daily Timescale for the Five Calibrated and Five Evaluated Sites (see Table 1)

Site	Function	Ecosystem type	Sample numbers	Willmott's index	R^2	ME
US-WPT	Calibration	Marsh	821	0.84	0.94	0.06
US-Tw1	Calibration	Marsh	1076	0.79	0.75	0.01
US-Myb	Evaluation	Marsh	1391	0.68	0.53	0.02
US-DPW	Evaluation	Marsh	460	0.76	0.77	0.08
US-OWC	Evaluation	Marsh	72	0.55	0.33	0.03
US-StJ	Calibration	Salt Marsh	270	0.45	0.13	0.04
US-LA1	Evaluation	Salt Marsh	193	0.50	0.2	0.13
US-Ho1	Calibration	Upland	552	0.24	0.15	0.01
US-CRT	Evaluation	Upland	346	0.22	0.15	0.01
US-Twt	Calibration	Rice	730	0.56	0.22	0.01

later time. The CH_4 flux by diffusion does not show a clear seasonality and contribute lesser CH_4 flux comparing to the other two pathways.

The intercomparison of model results with the coastal wetland salt marsh sites (US-LA1 and US-StJ) show overestimation of the coastal wetland CH_4 emissions without accounting for the reduction of methanogenesis caused by higher sulfate-reducing bacteria due to the saltwater intrusion (Figure 2f). After parameterizing this effect by calibrating the parameter $r_{\text{CH}_4:\text{CO}_2}$ value (0.03), modeled EM matches observations for the calibrated site (US-StJ; Figure 2f). While US-LA1 does not have a large impact from the tides, as reflected by low standard deviation from the observation, the calibrated site US-StJ results show a better Willmott's Index and R^2 but higher ME due to higher coastal tide effect, which ISAM does not account for. The impacts of the tide and salt water intrusion during summer leads to lower CH_4 emissions, which model is able to capture reasonably well. However, as Figure 2f shows, model is unable to capture late-season high CH_4 fluxes at this site, suggesting that causes of the higher CH_4 emission in later winter at US-StJ site cannot be solely explained by the changes in salinity and tides. These high emissions have not been discussed in the published literature. While our understating of changes in salt water marsh cycling due to changes in biochemical and environmental variables remain limited, a recent study (Huertas et al., 2019) has discussed two additional sources of CH_4 which may lead to higher CH_4 emissions: (1) lateral transport of nearby freshwater CH_4 through riverine overflow and (2) sedimentary methanogenesis. In an earlier study, the higher winter rates were hypothesized to be caused by the release of readily metabolized organic substrates as marsh plants mature and die (Bartlett et al., 1987).

Regarding two upland sites, one calibrated (US-Ho1) and another one evaluated (US-CRT) site, both sites have a low ME value, suggesting the model is able to capture the magnitude of CH_4 emission, but the low Willmott's Index and R^2 values describing a relatively poor representation of the seasonal variation of CH_4 emission. There could be several reasons for such low performance of the model. Since the CH_4 emission/sink from the upland ecosystem is sensitive to the soil hydrology, the seasonality of water table depth is critical for CH_4 emission, which depends on soil texture and porosity. For example, soils with higher clay percentage tend to create fewer oxygen microsites (Wagner, 2017) and to increase methanogenic activity by decreasing permeability, increasing soil stratification, and anaerobic conditions. However, higher soil clay percentage also adsorbs more substrate, which prevents methanogenesis, and thus reduce the CH_4 production (Segers, 1998). The net effect of soil clay contents on methanogenesis depends on the relative magnitude of these two opposite effects. However, two upland FLUXNET sites do not provide texture and porosity profile information. Therefore, we use the global dataset (GSDE) for these variables (Table 1). In addition, the emissions are impacted by the site history and the heterogeneity of the landscape nearby, as the site could be a drained swamp, which is the case for US-CRT (Chu et al., 2014). Overall, without considering the detailed site-specific information, the model is not able to capture observed seasonal variations in the soil moisture for these two upland sites. Therefore, the estimated Willmott's index and R^2 values for these two upland sites are low.

For the calibrated rice site (Us-Twt), the seasonal variation of CH_4 emission is primarily controlled by the specific rice phenology (Knox et al., 2016), thus producing several emission peaks during each year

Table 4

ISAM Estimated Annual-Mean Net CH₄ Emissions (EM) Over the CONUS, and Its Breakdown Into the Three Transport Mechanisms—Aerenchyma (A), Ebullition (E), and Diffusion (FD)—in TgCH₄ yr⁻¹ for the 2000s and 2090s Under RCP4.5 and RCP8.5 Future scenario

Year	Wetlands				Nonwetlands				Total			
	N_w	A_w	E_w	FD_w	N_{nw}	A_{nw}^a	E_{nw}	FD_{nw}	EM	A	E	FD
2000s	15.3	6.5	2.8	6.0	-1.5	0.7	0	-2.2	13.8	7.2	2.8	3.8
2090s (RCP4.5)	19.4	7.9	3.3	8.2	-1.5	1.3	0	-2.8	17.9	9.2	3.3	5.4
2090s (RCP8.5)	24.7	9.9	4.8	10.0	-2.1	1.9	0	-4.0	22.6	11.8	4.8	6.0

Note. The contributions from the wetlands (subscript *w*) and nonwetlands (subscript *nw*) are reported separately. Positive values represent a CH₄ emission to the atmosphere.

^a A_{nw} occurs when the soils are wet as also shown in the observation study (Jackson & Armstrong, 1999).

growing season. The model accounts for six phenological stages of rice growth (Lin et al., 2017), which help to produce seasonal emissions that are consistent with the observation, although the model is not able to reproduce peak emissions during the autumn of 2013, which is similar to the results of the nearby marsh site (US-Tw1), that a drastic increase of ebullition after the growing season can explain this finding, while other carbon fluxes and environmental variables are not able to explain this large interannual variability of CH₄ emission (Knox et al., 2016).

CH₄ emissions/sinks from the upland ecosystems are also sensitive to the soil hydrology. The seasonality of water table depth (which depends on soil texture and porosity) drives the seasonality of CH₄ emissions. For example, soil with high clay percentage tends to adsorb more substrate and prevent methanogenesis, and thus decrease the CH₄ production. However, FLUXNET sites do not provide texture and porosity profile information. Therefore, we applied the global dataset (GSDE) for these input variables (Table 1).

5.2. Historical Soil CH₄ Emissions Across the CONUS, 2001–2010

ISAM-estimated net emission EM over the 2000s is 13.8 TgCH₄ yr⁻¹ (Table 4), which is the sum of wetland total flux $N_w = 15.3$ TgCH₄ yr⁻¹ and nonwetland total flux $N_{nw} = -1.5$ TgCH₄ yr⁻¹ across the CONUS. Marsh and salt marsh wetlands contribute 60% and 40% of total modeled wetland emissions. Wetland CH₄ production P was 15.5 TgCH₄ yr⁻¹ (Figure S2), a slightly higher value than N_w , suggesting almost all wetland production is emitted to the atmosphere via the three emission pathways, FD (39%), A (43%), and E (18%) over the decade. If the effects of salt water intrusion and sea level rise on coastal wetlands are not included, the ISAM-estimated EM and N_w for the 2000s would be 20.7 and 22.2 TgCH₄ yr⁻¹, or about 49% and 44% higher respectively, a proof of the importance of including these effects.

Nonwetland grid cells with higher P_{nw} in anaerobic microsites than O_{nw} contributed 1.4 TgCH₄ yr⁻¹ soil emissions, whereas grid cells with higher O_{nw} than P_{nw} contributed -2.9 TgCH₄ yr⁻¹ soil sinks, and so overall the nonwetland is a net sink of CH₄ over the CONUS.

ISAM calculated the spatial pattern of wetland flux N_w over the CONUS region (Figure 4a) shows higher emissions in the eastern and southeastern coastal regions, Mississippi River Delta zone, and near Lake Superior. While increasing wetland extent (Figure 3a) is the major cause of higher emissions, a higher temperature is an additional factor contributing to higher emissions, because methanogens in warm and moist environments consume soil carbon more rapidly. Grid cells with the same wetland fraction but higher temperatures show higher N_w (Figure S3). This effect is stronger when the wetland extent is 0.4 or less.

The majority of nonwetlands in the midwest, northeast, and Mississippi River delta zone shown in Figure 4d are a net source of N_{nw} for the 2000s with A_{nw} and FD_{nw} each contributed approximately 50% to the total transport of these emissions from the soil column to the atmosphere. Other nonwetland regions, especially the Rocky and Appalachian mountainous, are a net sink for N_{nw} in Figure 4d.

Both P_{nw} and O_{nw} are important determinants for the overall pattern of N_{nw} . Soil moisture of the top 30 cm is the dominant factor impacting P_{nw} and O_{nw} and determining whether the soil is a CH₄ source or sink (Figure S4). For regions with soil moisture higher than 50% (Figure S4), such as the U.S. Midwest and the coastal region of Northeastern CONUS (Box (a) in Figure S5), both P_{nw} (Figure S6d) and O_{nw} (Figure S6g) are higher, but P_{nw} exceeds O_{nw} because of colder temperatures (Figure S4) and nonwetland soil is a

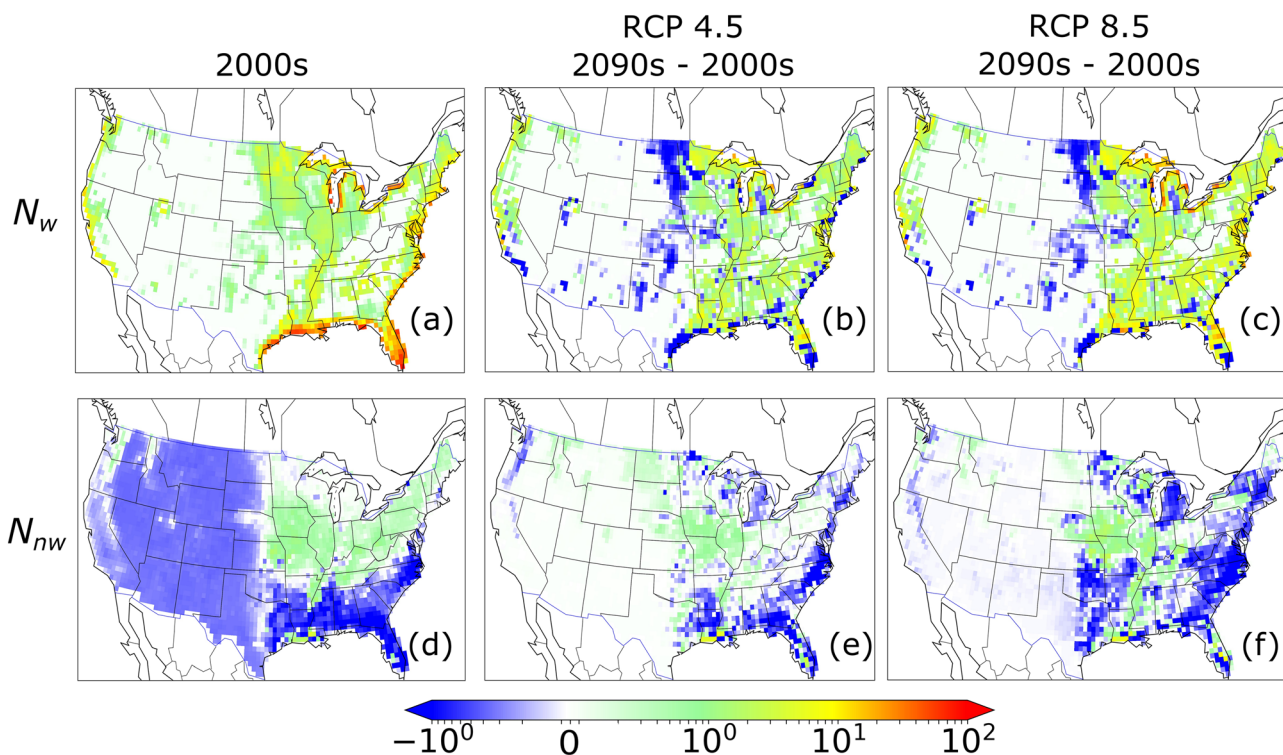


Figure 4. ISAM-estimated decadal-mean CH_4 flux ($\text{gCH}_4 \text{ m}^{-2} \text{ yr}^{-1}$) for wetlands (N_w) (Row 1) and for nonwetlands (N_{nw}) (Row 2) over the 2000s (a, d); the change from the 2000s to the 2090s under the RCP4.5 climate scenario (b, e) and under the RCP8.5 climate scenario (c, f). Note that the color bar legend shows a broken logarithmic scale for the net flux of CH_4 to the atmosphere including negative values, which represent CH_4 uptake by soils in panels (a) and (d) or a decrease in flux for some areas in panels (b, c, e, and f).

source. In regions with soil moisture lower than 50%, such as the large mountainous region in the western CONUS (Box (b) in Figure S5), O_{nw} (Figure S6g) is many times larger than P_{mw} (Figure S6d). Thus, nonwetland soil is a sink for atmospheric CH_4 (Figure S4).

Of the three transport mechanisms for wetland and nonwetland combined, we find A ($7.2 \text{ TgCH}_4 \text{ yr}^{-1}$) to be the largest contributor to the transport of total CH_4 (i.e., wetland + nonwetland) to the atmosphere (Table 4). Wetland regions with high A are in the southern CONUS where vascular plants with higher aerenchyma were prevalent, such as shrubs and forests. In addition, the higher temperature also increases the plant activity and thus A . The contribution of FD to EM is the second largest of the CONUS ($3.8 \text{ TgCH}_4 \text{ yr}^{-1}$) and is the dominant transport mechanism emissions for seasonal wetlands and nonwetland regions (Figure 5b). FD is the only transport mechanism for soil CH_4 uptake (i.e., negative EM) in the nonwetland western CONUS and the southeastern mountainous region, because these regions have a deeper water table depth. Transport by E ($2.8 \text{ TgCH}_4 \text{ yr}^{-1}$) is the smallest and is limited to wetland regions with high temperature, especially in the southeastern coastal region of the CONUS (Figure 5c).

5.3. Future Soil CH_4 Emissions Across the CONUS, 2011–2,100

In future climate scenarios, the increases in temperature and wetland extent lead to increases in EM . By the 2090s, the expansion of the wetland extent (from 0.45 to 0.48 Mkm^2 under RCP4.5 and 0.49 Mkm^2 under RCP8.5) caused by higher precipitation and sea level rise contributes to higher P (Figures 5k and 5q). Thus, EM is higher under two future climate scenarios. ISAM estimated EM under two scenarios ranges 17.9 – $22.6 \text{ TgCH}_4 \text{ yr}^{-1}$ (RCP4.5–RCP8.5) by the 2090s, which are about 32–87% higher than the 2000s EM (Table 4). Increase in P_{mw} (8.7 – $17.4 \text{ TgCH}_4 \text{ yr}^{-1}$) is much higher than the increase in P_w (4.5 – $9.8 \text{ TgCH}_4 \text{ yr}^{-1}$) by the 2090s (Figure S2). However, O_{mw} also increases at higher rates (9.9 – $20 \text{ TgCH}_4 \text{ yr}^{-1}$), resulting in the overall increase in EM under two scenarios.

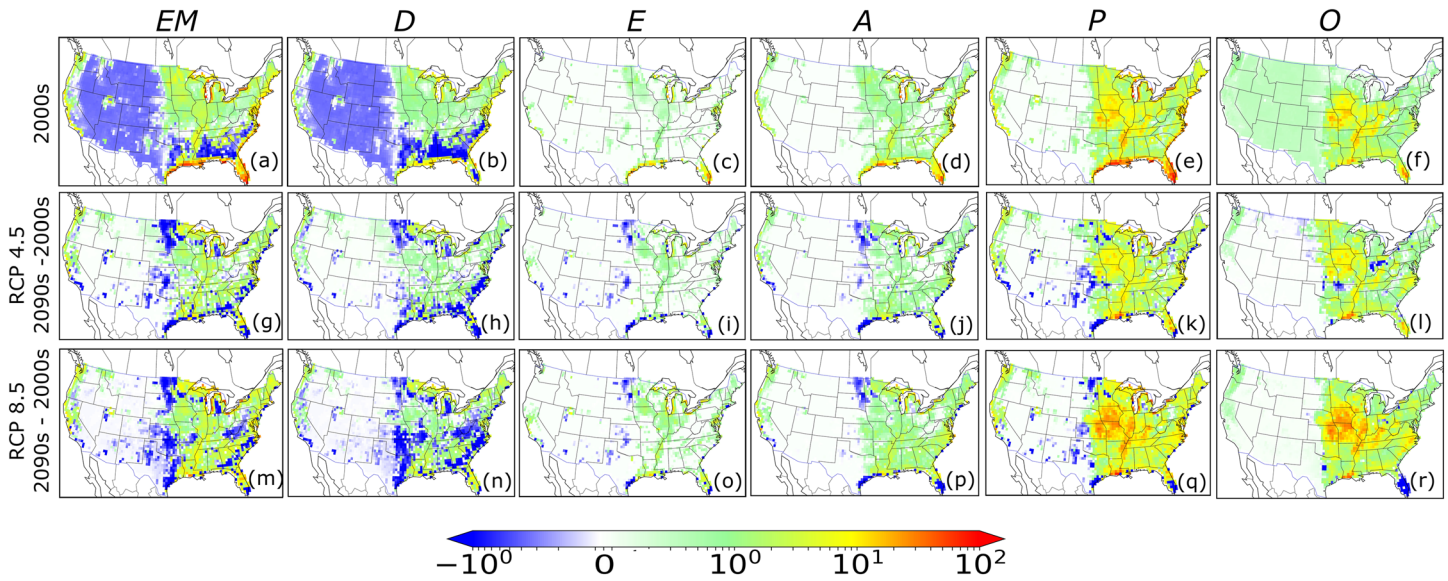


Figure 5. ISAM-estimated decadal-mean CH_4 flux ($\text{gCH}_4 \text{ m}^{-2} \text{ yr}^{-1}$) to the atmosphere, $EM = N_w + N_{nw}$ (Column 1), ISAM-estimated contributions to EM from the three transport mechanisms: Diffusion (FD , Column 2), ebullition (E , Column 3) and aerenchyma transport (A , Column 4), and decadal-mean CH_4 production (P , Row 5) and oxidation (O , Row 6) integrated over the soil column over the 2000s (a–f); the change from the 2000s to the 2090s under the RCP4.5 climate scenario (g–l) and under the RCP8.5 climate scenario (m–r). Note that all colors are plotted using a logarithmic scale. The color bar legend shows a broken logarithmic scale, including both positive and negative values for all of the panels.

N_w is the major contributor to the increase in EM under both scenarios ($19.4\text{--}24.7 \text{ TgCH}_4 \text{ yr}^{-1}$) by the 2090s due to wetter and warmer conditions. Note that if the effect of salt water intrusion were not accounted for, these emissions would have been increased by 23–27%, and sea level rise by 2% and 4% under two scenarios.

There is no clear spatial pattern of N_w change found, except for the higher increase values in N_w in the northwestern and southeastern CONUS (Figures 4b and 4c) due to both the large increase in the wetland extent (Figures 3b and 3c) in these areas.

Of the three different transport pathways (A , E , and FD), the increase in A_w along northern Great lakeshore and in the southern CONUS under both scenarios is the primary contributor to the larger N_w (Table 4 and Figures 5j and 5p), mainly due to an increase in biomass as a result of both the warmer climate and the CO_2 fertilization effect. On the other hand, an increase in E (or E_w) under RCP4.5 by the 2090s is much smaller (19% relative to the 2000s) than under RCP8.5 (78% relative to the 2000s) (Table 4 and Figures 5i and 5o). E is higher mainly in productive wetlands (Table 4), because of higher CH_4 concentration due to higher methanogenesis through higher litter input, and thus greater bubble formation. The larger increase in the productive land under RCP8.5 by the 2090s is the result of a larger increase in the wetland area extent, especially the increase in fractional water near the eastern coastal region and the Mississippi Delta (Figures 3b and 3c). Warmer temperature decreases the CH_4 solubility in the soil water thus increases E , but this increase in CH_4 emissions is smaller compared to the increase in N_w due to the expansion of the wetland extent. The increase of FD is relatively small as compared to A under both scenarios partly due to FD_{nw} , that is the diffusion of atmospheric CH_4 to the soils (Table 4), and the small response of FD_w for both future climate scenarios by the 2090s, because of the drier topsoil and lower CH_4 production.

The nonwetland N_{nw} contributes a small sink to EM under both scenarios (RCP4.5–RCP8.5) by the 2090s (Table 4). The increase in CH_4 sinks is larger than the CH_4 sources by the 2090s. Overall, the net CH_4 sink from the nonwetland region becomes larger under both scenarios by the 2090s, but still is less than 10% of EM .

The spatial patterns of N_{nw} under both scenarios show a transition from CH_4 source to sink in the northeastern CONUS (Figures 4e and 4f) compare to the pattern over the 2000s, because of the reduction of the soil moisture over this region under the future climate projections. As for the aerenchyma transport pathway

(i.e., A_{mw}), our model results show that it is almost doubled under RCP4.5 and tripled under RCP8.5 (Table 4), despite the fact that the soil moisture is decreased under future scenarios. This is because aerenchyma transport is also positively correlated with the plant productivity and leaf area index (Wania et al., 2010) (see model Equations S1.24–S1.26). ISAM results show that plant productivity (and leaf area index) increases, and soil moisture decreases under future scenarios. Overall, the effect on A_{mw} of increase productivity outweighs that of reduced soil moisture. The FD_{mw} from the atmosphere to the soil column is also increased, mostly due to the increase in temperature.

6. Comparison of ISAM Results With Other Studies

Note that we compare ISAM-estimated N_w with other model results, because most of the reported results are only for N_w (Table 5). Tian et al. (2012) did provide an estimate of the CH₄ sink across the CONUS of 1.3 TgCH₄ yr⁻¹, slightly lower than the ISAM estimates of 1.5 TgCH₄ yr⁻¹. Our model also reflects a good match to the previous publications of the hotspot regions for CH₄ emission (Bloom et al., 2017; Potter et al., 2006; Saunio et al. 2016; Tian et al., 2010), and these include southeastern CONUS, Mississippi delta, Western coast, and the Upper Midwest. Among these regions, the southeastern CONUS contributes the largest emission due to the higher temperature. All the hotspot regions contain a certain fraction of the saline wetland except the Upper Midwest.

In particular, ISAM-estimated spatial distribution for N_w is consistent with the WetCHARTs product (Figure S7), except for the Midwest region, where ISAM N_w shows the seasonal wetland area contributed substantially to N_w , while WetCHARTs product shows almost negligible emission from this region. In spite of the similarity between ISAM and WetCHARTs results, there are various differences between the two studies. First, while the annual mean values for the wetland extent for the 2000s used in ISAM are lower (0.45 Mkm²) than WetCHARTs product (0.47 Mkm²), the SWAMPs product used in this study shows a higher seasonal wetland extent areas, particularly in the Midwest region, compared to WetCHARTs product. This difference has led to higher wetland emissions over the Midwest in ISAM case. Second, ISAM omitted anaerobic oxidation in wetlands, especially in the coastal wetlands, resulting in the lower N_w . Third, ISAM uses a higher Q_{10} value of 2.2 (which we had calibrated with site-level data) compared to other studies (Riley et al., 2011; Wania et al., 2010), which use a Q_{10} of 2. With slightly higher Q_{10} , ISAM does estimate higher N_w (Table S4). For example, ISAM estimates a higher N_w in the warmer eastern coastal region, but a lower N_w in the inland western CONUS (Figure S7). Fourth, a vertically resolved soil biogeochemistry component of ISAM calculates soil heterotrophic respiration and thus P for each soil layer up to 3.5 m and thus estimates additional N_w from deeper soil layers. For example, ISAM-estimated N_w based on first 0.3 m soil (five soil layers) were about 2.5 TgCH₄ yr⁻¹ lesser than estimated based on 3.5-m soil (Table S4). Fifth, ISAM also accounts for the effect of salt water intrusion on methanogenesis along the coastlines. This effect alone reduced the ISAM-estimated CH₄ emissions for the 2000s by 6.9 TgCH₄ yr⁻¹ (the difference between with and without coastal wetland effect, Table 4). Finally, ISAM calibrated $r_{CH_4:CO_2}$ for the freshwater wetlands is about 0.06 compared to a published range of 0.0001–0.1 and median of 0.04, which are estimated based on the multiple freshwater wetland sites (Segers, 1998). When calculations were performed with $r_{CH_4:CO_2}$ of 0.04 for freshwater, the ISAM estimated N_w turned out to be about 14.8 TgCH₄ yr⁻¹. This result is consistent with the mean of the WetCHARTs product value (14.8 TgCH₄ yr⁻¹, Table 5). However, with the coastal wetland effect, ISAM would have an estimated lower N_w than WetCHARTs product value.

We also compared ISAM estimated soil CH₄ uptake from the dry or upland soils (i.e., mainly FD for the dry soils) for a Colorado State measurement site studied by Curry (2007). ISAM estimated CH₄ uptake for this site is 0.3 gCH₄ m⁻² yr⁻¹, which exactly matched with the Curry (2007) observation-based estimate. ISAM estimated spatial pattern of FD for the upland (Figure 5b) across the CONUS shows the highest uptake in the mountainous region and southwest, where soil moisture is low and soil pores are aerated well, which also matches well with the conclusions of the previous studies (Curry, 2007; Tian et al., 2016). Soil emperature is another factor determining the dry soil CH₄ uptake rate. For example, compared to the colder Midwest region, higher soil uptake is found in the upland soils between northeastern and southeastern areas due to their warmer temperature increasing methanotroph activity in dry soils and thus increasing the soil sink.

Table 5

Published Estimation of Soil CH₄ Emission, Sink, and Net Flux (Unit: TgCH₄yr⁻¹) for the CONUS. Numbers in the Parentheses Show The Uncertainty Range of Soil CH₄ Emission, Sink, and Net Flux.

Soil CH ₄ flux	This study		Potter et al. (2006)	Xu et al. (2010)	Tian et al. (2010)	Tian et al. (2012)	Saunois et al. (2016)	Bloom et al. (2017)
	With coastal wetland effect	Without coastal wetland effect						
Emission	15.3	22.2	5.5			6.2 (3.3–9.1)	14.3 (5.5–23.0)	14.9 (8.3–27.3)
Sink	1.5	1.5				1.31		
Net flux	13.8	20.7		7.25	7.2 ± 0.6			

There is no other modeling study available in the literature on future CH₄ scenario analysis for the CONUS that we can compare with our model results directly. Zhang et al. (2017), however, performed simulation using a simple algorithm to calculate CH₄ emission from wetlands at a global total case and found an increase in global total CH₄ emissions by 20% under RCP4.5 and 70% under RCP8.5. Our modeling study also shows similar CH₄ emissions increasing trends under the two scenarios across the CONUS (Table 4).

7. Conclusions

A newly developed vertically resolved soil CH₄ dynamics module has been coupled to a land surface model, ISAM. After calibrating and evaluating ISAM using site-level soil CH₄ emissions data, the model is applied to calculate CH₄ emissions and sinks from wetlands and nonwetland soils across the CONUS over historical time and under two future scenarios.

ISAM-estimated *EM* across the CONUS for the 2000s is 13.8 Tg CH₄ yr⁻¹. The results show that wetlands, including seasonal wetlands, dominate soil CH₄ emissions ($N_w = 15.3$ Tg CH₄ yr⁻¹), mainly in the eastern and southeastern coastal regions, Mississippi River delta zone and the regions near Lake Superior.

Model-estimated future *EM* under RCP4.5 and RCP8.5 scenarios by the 2090s were about 30% and 64% higher than over the 2000s, mostly due to an increase in temperature and an increase in seasonal wetland extent due to higher precipitation. The overall increase in CH₄ emissions under two future scenarios suggests positive feedback in the climate system with increases in radiative forcing leading to higher CH₄ emissions.

In contrast to wetland emissions, nonwetland soils were estimated to be a small CH₄ sink ($N_{nw} = -1.5$ Tg CH₄ yr⁻¹) for the 2000s, and this sink increased by 17% and 58% by the 2090s under RCP4.5 and RCP8.5 scenarios. Overall, the magnitude of N_{nw} is less than 10% of *EM*.

We find that the strength of different CH₄ transport mechanisms differs across wetlands and nonwetland soils, and they are sensitive to environmental conditions. Diffusion dominates in nonwetland soils with low soil moisture, whereas ebullition is more important in wetlands, and aerenchyma transport is important in both wetlands and nonwetlands. Under future scenarios, ISAM simulations show higher CH₄ emissions, which are mainly transported by ebullition due to the increase in wetland extent and by increased aerenchyma transport caused by aerenchyma growth due to the CO₂ fertilization effect.

This is the first study that estimates CH₄ emissions and sinks not only from wetlands (including freshwater and coastal wetlands) but also from the nonwetland soils (including wet and dry soils) under future climate scenarios across the CONUS. Applying this approach to soils worldwide, could provide the information needed to make quantitative estimates of the strength of the climate feedback between climate change and soil CH₄ emissions. To do this, there is a need for additional CH₄ emission modeling analyses from wetlands and nonwetland soils for other regions ranging from the arctic to the tropics.

Data Availability Statement

The estimates of annual mean wetlands and nonwetlands CH₄ emissions for the CONUS region using ISAM under three cases: (1) 2001–2010, (2) 2091–2,100 under RCP4.5, and (3) 2091–2,100 under RCP8.5 scenarios can be downloaded for free from the ISAM website (<http://climate.atmos.uiuc.edu/Methane>). The data files

contain the following methane fluxes for both wetlands and nonwetlands soils: (1) CH₄ emission, (2) CH₄ production, (3) soil CH₄ oxidation, (4) CH₄ emissions through aerenchyma transport, (5) CH₄ emissions through ebullition, and (6) CH₄ emissions/sink through diffusion. The wetland extent described by the fractional area of surface water is also stored. We are sharing the data at 30 m spatial resolution at 0.5 × 0.5° resolution. All the data are stored in NetCDF files. The data can be accessed from the ISAM website (http://climate.atmos.uiuc.edu/Methane_ShueEtAl/).

Acknowledgments

The output of all model results discussed in this paper and listed in the Data Availability Statement section is available for download from the ISAM website (http://climate.atmos.uiuc.edu/Methane_ShueEtAl/).

References

- Adamsen, A. P. S., & King, G. M. (1993). Methane consumption in temperate and subarctic forest soils: Rates, vertical zonation, and responses to water and nitrogen. *Applied and Environmental Microbiology*, *59*(2), 485–490. <https://doi.org/10.1128/AEM.59.2.485-490.1993>
- Ahlström, A., Raupach, M. R., Schurgers, G., Smith, B., Arneeth, A., Jung, M., et al. (2015). The dominant role of semi-arid ecosystems in the trend and variability of the land CO₂ sink. *Science*, *348*(6237), 895–899. <https://doi.org/10.1126/science.aaa1668>
- Angle, J. C., Morin, T. H., Solden, L. M., Narrowe, A. B., Smith, G. J., Borton, M. A., et al. (2017). Methanogenesis in oxygenated soils is a substantial fraction of wetland methane emissions. *Nature Communications*, *8*, 1567. <https://doi.org/10.1038/s41467-017-01753-4>
- Baldocchi, D., Knox, S., Dronova, I., Verfaillie, J., Oikawa, P., Sturtevant, C., et al. (2016). The impact of expanding flooded land area on the annual evaporation of rice. *Agricultural and Forest Meteorology*, *223*, 181–193. <https://doi.org/10.1016/j.agrformet.2016.04.001>
- Barman, R., & Jain, A. K. (2016). Comparison of effects of cold-region soil/snow processes and the uncertainties from model forcing data on permafrost physical characteristics. *Journal of Advances in Modeling Earth Systems*, *8*, 453–466. <https://doi.org/10.1002/2015MS000504>
- Barman, R., Jain, A. K., & Liang, M. (2014a). Climate-driven uncertainties in terrestrial gross primary production: A site-level to global scale analysis. *Global Change Biology*, *20*, 944–953. <https://doi.org/10.1111/gcb.12474>
- Barman, R., Jain, A. K., & Liang, M. (2014b). Climate-driven uncertainties in terrestrial energy and water fluxes: A site-level to global scale analysis. *Global Change Biology*, *20*, 1885–1900. <https://doi.org/10.1111/gcb.12473>
- Bartlett, K. B., Bartlett, D. S., Harriss, R. C., & Sebachner, D. I. (1987). Methane emissions along a salt marsh salinity gradient. *Biogeochemistry*, *4*(3), 183–202. <https://doi.org/10.1007/BF02187365>
- Bhullar, G. S., Edwards, P. J., & Olde Venterink, H. (2013). Variation in the plant-mediated methane transport and its importance for methane emission from intact wetland peat mesocosms. *Journal of Plant Ecology*, *6*(4), 298–304. <https://doi.org/10.1093/jpe/rts045>
- Bloom, A. A., Bowman, K. W., Lee, M., Turner, A. J., Schroeder, R., Worden, J. R., et al. (2017). A global wetland methane emissions and uncertainty dataset for atmospheric chemical transport models (WetCHARTs version 1.0). *Geoscientific Model Development*, *10*(6), 2141–2156. <https://doi.org/10.5194/gmd-10-2141-2017>
- Cao, M., Gregson, K., & Marshall, S. (1998). Global methane emission from wetlands and its sensitivity to climate change. *Atmospheric Environment*, *32*(19), 3293–3299. [https://doi.org/10.1016/S1352-2310\(98\)00105-8](https://doi.org/10.1016/S1352-2310(98)00105-8)
- Chu, H., Chen, J., Gottgens, J. F., Ouyang, Z., John, R., Czajkowski, K., & Becker, R. (2014). Net ecosystem methane and carbon dioxide exchanges in a Lake Erie coastal marsh and a nearby cropland. *Journal of Geophysical Research: Biogeosciences*, *119*, 722–740. <https://doi.org/10.1002/2013JG002520>
- Chu, H., Gottgens, J. F., Chen, J., Sun, G., Desai, A. R., Ouyang, Z., et al. (2015). Climatic variability, hydrologic anomaly, and methane emission can turn productive freshwater marshes into net carbon sources. *Global Change Biology*, *21*, 1165–1181. <https://doi.org/10.1111/gcb.12760>
- Curry, C. L. (2007). Modeling the soil consumption of atmospheric methane at the global scale. *Global Biogeochemical Cycles*, *21*, GB4012. <https://doi.org/10.1029/2006GB002818>
- Dlugokenky, E. J. (2018). NOAA Earth System Research Laboratory Global Monitoring Division-Global Greenhouse Gas Reference Network: Trends in atmospheric methane. Retrieved from https://www.esrl.noaa.gov/gmd/ccgg/trends_ch4/
- El-Masri, B., Barman, R., Meiyappan, P., Song, Y., Liang, M., & Jain, A. K. (2013). Carbon dynamics in the Amazonian basin: Integration of eddy covariance and ecophysiological data with a land surface model. *Agricultural and Forest Meteorology*, *182–183*, 156–167.
- El-Masri, B., Shu, S., & Jain, A. K. (2015). Implementation of a dynamic rooting depth and phenology into a land surface model: Evaluation of carbon, water, and energy fluxes in the high latitude ecosystems. *Agricultural and Forest Meteorology*, *211–212*, 85–99. <https://doi.org/10.1016/j.agrformet.2015.06.002>
- Elzein, A., & Balesdent, J. (1995). Mechanistic simulation of vertical distribution of carbon concentrations and residence times in soils. *Soil Science Society of America Journal*, *59*(5), 1328–1335. <https://doi.org/10.2136/sssaj1995.03615995005900050019x>
- Gahlot, S., Shu, S., Jain, A. K., & Roy, S. B. (2017). Estimating trends and variation of net biome productivity in India for 1980–2012 using a land surface model. *Geophysical Research Letters*, *44*, 11,573–11,579. <https://doi.org/10.1002/2017GL075777>
- Giri, C., Ochieng, E., Tieszen, L. L., Zhu, Z., Singh, A., Loveland, T., et al. (2011). Status and distribution of mangrove forests of the world using Earth observation satellite data. *Global Ecology and Biogeography*, *20*(1), 154–159. <https://doi.org/10.1111/j.1466-8238.2010.00584.x>
- Harris, I. P. D. J., Jones, P. D., Osborn, T. J., & Lister, D. H. (2014). Updated high-resolution grids of monthly climatic observations—the CRU TS3. 10 dataset. *International Journal of Climatology*, *34*(3), 623–642. <https://doi.org/10.1002/joc.3711>
- Huertás, I. E., de la Paz, M., Perez, F. F., Navarro, G., & Flecha, S. (2019). Methane emissions from the salt marshes of Doñana wetlands: Spatio-temporal variability and controlling factors. *Frontiers in Ecology and Evolution*, *7*, 32–32. <https://doi.org/10.3389/fevo.2019.00032>
- Huntzinger, D. N., Michalak, A. M., Schwalm, C., Ciais, P., King, A. W., Fang, Y., et al. (2017). Uncertainty in the response of terrestrial carbon sink to environmental drivers undermines carbon-climate feedback predictions. *Scientific Reports*, *7*, 4765. <https://doi.org/10.1038/s41598-017-03818-2>
- Iversen, C. M., Childs, J., Norby, R. J., Ontl, T. A., Kolka, R. K., Brice, D. J., et al. (2018). Fine-root growth in a forested bog is seasonally dynamic, but shallowly distributed in nutrient-poor peat. *Plant and Soil*, *424*(1–2), 123–143. <https://doi.org/10.1007/s11104-017-3231-z>
- Jackson, M. B., & Armstrong, W. (1999). Formation of Aerenchyma and the processes of plant ventilation in relation to soil flooding and submergence. *Plant Biology*, *1*(3), 274–287. <https://doi.org/10.1111/j.1438-8677.1999.tb00253.x>
- Jain, A. K., Meiyappan, P., Song, Y., & House, J. (2013). CO₂ emissions from land-use change affected more by nitrogen cycle, than by the choice of land-cover data. *Global Change Biology*, *19*, 2893–2906. <https://doi.org/10.1111/gcb.12207>

- Jain, A. K., West, T. O., Yang, X., & Post, W. M. (2005). Assessing the impact of changes in climate and CO₂ on potential carbon sequestration in agricultural soils. *Geophysical Research Letters*, *32*, L19711. <https://doi.org/10.1029/2005GL023922>
- Jung, M., Reichstein, M., Schwalm, C. R., Huntingford, C., Sitch, S., Ahlström, A., et al. (2017). Compensatory water effects link yearly global land CO₂ sink changes to temperature. *Nature*, *541*(7638), 516–520. <https://doi.org/10.1038/nature20780>
- Kaiser, K. E., McGlynn, B. L., & Dore, J. E. (2018). Landscape analysis of soil methane flux across complex terrain. *Biogeosciences*, *15*(10), 3143–3167. <https://doi.org/10.5194/bg-15-3143-2018>
- Kirschke, S., Bousquet, P., Ciais, P., Saunois, M., Canadell, J. G., Dlugokencky, E. J., et al. (2013). Three decades of global methane sources and sinks. *Nature Geoscience*, *6*(10), 813–823. <https://doi.org/10.1038/ngeo1955>
- Knox, S. H., Dronova, I., Sturtevant, C., Oikawa, P. Y., Matthes, J. H., Verfaillie, J., & Baldocchi, D. (2017). Using digital camera and Landsat imagery with eddy covariance data to model gross primary production in restored wetlands. *Agricultural and Forest Meteorology*, *237–238*, 233–245. <https://doi.org/10.1016/j.agrformet.2017.02.020>
- Knox, S. H., Jackson, R. B., Poulter, B., McNicol, G., Fluet-Chouinard, E., Zhang, Z., et al. (2019). 0: FLUXNET-CH₄ synthesis activity: Objectives, observations, and future directions. *Bulletin of the American Meteorological Society*, *100*(12), 2607–2632. <https://doi.org/10.1175/BAMS-D-180268.1>
- Knox, S. H., Matthes, J. H., Sturtevant, C., Oikawa, P. Y., Verfaillie, J., & Baldocchi, D. (2016). Biophysical controls on interannual variability in ecosystem-scale CO₂ and CH₄ exchange in a California rice paddy. *Journal of Geophysical Research: Biogeosciences*, *121*, 978–1001. <https://doi.org/10.1002/2015JG003247>
- Krauss, K. W., From, A. S., Doyle, T. W., Doyle, T. J., & Barry, M. J. (2011). Sea-level rise and landscape change influence mangrove encroachment onto marsh in the ten Thousand Islands region of Florida, USA. *Journal of Coastal Conservation*, *15*(4), 629–638. <https://doi.org/10.1007/s11852-011-0153-4>
- Lamarque, J. F., Kyle, G. P., Meinshausen, M., Riahi, K., Smith, S. J., van Vuuren, D. P., et al. (2011). Global and regional evolution of short-lived radiatively-active gases and aerosols in the representative concentration pathways. *Climatic Change*, *109*(1–2), 191–212. <https://doi.org/10.1007/s10584-011-0155-0>
- Lawrence, D. M., & Slater, A. G. (2008). Incorporating organic soil into a global climate model. *Climate Dynamics*, *30*(2–3), 145–160. <https://doi.org/10.1007/s00382-007-0278-1>
- Le Quéré, C., Andrew, R. M., Friedlingstein, P., Sitch, S., Hauck, J., Pongratz, J., et al. (2018). Global carbon budget 2018. *Earth System Science Data*, *10*(4), 2141–2194. <https://doi.org/10.5194/essd-10-2141-2018>
- Lin, T.S., Jain, A.K., & Kheshgi, H.S., (2017). Studying the impacts of environmental factors and agricultural managements on the methane Emissions from Rice paddies using a land surface model, American Geophysical Union Fall 2017 Meeting, New Orleans, LA, 11–15 December 2017.
- Mao, J., Fu, W., Shi, X., Ricciuto, D. M., Fisher, J. B., Dickinson, R. E., et al. (2015). Disentangling climatic and anthropogenic controls on global terrestrial evapotranspiration trends. *Environmental Research Letters*, *10*, 094008. <https://doi.org/10.1088/1748-9326/10/9/094008>
- Matthes, J. H., Sturtevant, C., Verfaillie, J., Knox, S., & Baldocchi, D. (2014). Parsing the variability in CH₄ flux at a spatially heterogeneous wetland: Integrating multiple eddy covariance towers with high-resolution flux footprint analysis. *Journal of Geophysical Research: Biogeosciences*, *119*, 1322–1339. <https://doi.org/10.1002/2014JG002642>
- Matthews, E., & Fung, I. (1987). Methane emission from natural wetlands: Global distribution, area, and environmental characteristics of sources. *Global Biogeochemical Cycles*, *1*(1), 61–86. <https://doi.org/10.1029/GB001i001p00061>
- Meiyappan, P., & Jain, A. K. (2012). Three distinct land-cover estimates of historical land-cover change and land use conversions over the period of 200 years. *Frontier of Earth Sciences*, *6*(2), 122–139. <https://doi.org/10.1007/s11707-012-0314-2>
- Meiyappan, P., Jain, A. K., & House, J. I. (2015). Increased influence of nitrogen limitation on CO₂ emissions from future land use and land use change. *Global Biogeochemical Cycles*, *29*, 1524–1548. <https://doi.org/10.1002/2015GB005086>
- Miller, D. A., & White, R. A. (1998). A conterminous United States multilayer soil characteristics dataset for regional climate and hydrology Modeling. *Earth Interactions*, *2*(2), 1–26. [https://doi.org/10.1175/1087-3562\(1998\)002<0001:ACUSMS>2.3.CO;2](https://doi.org/10.1175/1087-3562(1998)002<0001:ACUSMS>2.3.CO;2)
- Millington, R. J., & Quirk, J. P. (1961). Permeability of porous solids. *Transactions of the Faraday Society*, *57*, 1200–1207. <https://doi.org/10.1039/tf9615701200>
- Moldrup, P., Yoshikawa, S., Olesen, T., Komatsu, T., & Rolston, D. E. (2003). Air permeability in undisturbed volcanic ash soils. *Soil Science Society of America Journal*, *67*(1), 32–40.
- Ni, X., & Groffman, P. M. (2018). Declines in methane uptake in forest soils. *Proceedings of the National Academy of Sciences*, *115*(34), 8587–8590. <https://doi.org/10.1073/pnas.1807377115>
- Oikawa, P. Y., Jenerette, G. D., Knox, S. H., Sturtevant, C., Verfaillie, J., Dronova, I., et al. (2017). Evaluation of a hierarchy of models reveals importance of substrate limitation for predicting carbon dioxide and methane exchange in restored wetlands. *Journal of Geophysical Research: Biogeosciences*, *122*, 145–167. <https://doi.org/10.1002/2016JG003438>
- Olefeldt, D., Turetsky, M. R., Crill, P. M., & McGuire, A. D. (2013). Environmental and physical controls on northern terrestrial methane emissions across permafrost zones. *Global Change Biology*, *19*, 589–603. <https://doi.org/10.1111/gcb.12071>
- Poffenbarger, H. J., Needelman, B. A., & Megonigal, J. P. (2011). Salinity influence on methane emissions from tidal marshes. *Wetlands*, *31*(5), 831–842. <https://doi.org/10.1007/s13157-011-0197-0>
- Portmann, F. T., Siebert, S., & Döll, P. (2010). MIRCA2000—Global monthly irrigated and rainfed crop areas around the year 2000: A new high-resolution data set for agricultural and hydrological modeling. *Global Biogeochemical Cycles*, *24*, GB1011. <https://doi.org/10.1029/2008GB003435>
- Potter, C., Klooster, S., Hiatt, S., Fladeland, M., Genovese, V., & Gross, P. (2006). Methane emissions from natural wetlands in the United States: Satellite-derived estimation based on ecosystem carbon cycling. *Earth Interactions*, *10*(22), 1–12. <https://doi.org/10.1175/EI2006.1>
- Ren, X., Weitzel, M., O'Neill, B. C., Lawrence, P., Meiyappan, P., Levis, S., et al. (2018). Avoided economic impacts of climate change on agriculture: Integrating a land surface model (CLM) with a global economic model (iPETS). *Climatic Change*, *146*(3–4), 517–531. <https://doi.org/10.1007/s10584-016-1791-1>
- Rey-Sanchez, A. C., Morin, T. H., Stefanik, K. C., Wrighton, K., & Bohrer, G. (2018). Determining total emissions and environmental drivers of methane flux in a Lake Erie estuarine marsh. *Ecological Engineering*, *114*, 7–15. <https://doi.org/10.1016/j.ecoleng.2017.06.042>
- Riley, W. J., Subin, Z. M., Lawrence, D. M., Swenson, S. C., Torn, M. S., Meng, L., et al. (2011). Barriers to predicting changes in global terrestrial methane fluxes: Analyses using CLM4Me, a methane biogeochemistry model integrated in CESM. *Biogeosciences*, *8*(7), 1925–1953. <https://doi.org/10.5194/bg-8-1925-2011>
- Saunois, M., Bousquet, P., Poulter, B., Pregon, A., Ciais, P., Canadell, J. G., et al. (2016). The global methane budget 2000–2012. *Earth System Science Data*, *8*(2), 697–751. <https://doi.org/10.5194/essd-8-697-2016>

- Schaefer, K., Schwalm, C. R., Williams, C., Arain, M. A., Barr, A., Chen, J. M., et al. (2012). A model-data comparison of gross primary productivity: Results from the north American carbon program site synthesis. *Journal of Geophysical Research*, *117*, G03010.
- Schroeder, R., McDonald, K. C., Chapman, B. D., Jensen, K., Podest, E., Tessler, Z. D., et al. (2015). Development and evaluation of a multi-year fractional surface water data set derived from active/passive microwave remote sensing data. *Remote Sensing*, *7*(12), 16,688–16,732. <https://doi.org/10.3390/rs71215843>
- Schuerch, M., Spencer, T., Temmerman, S., Kirwan, M. L., Wolff, C., Lincke, D., et al. (2018). Future response of global coastal wetlands to sea-level rise. *Nature*, *561*(7722), 231–234. <https://doi.org/10.1038/s41586-018-0476-5>
- Segers, R. (1998). Methane production and methane consumption: A review of processes underlying wetland methane fluxes. *Biogeochemistry*, *41*(1), 23–51. <https://doi.org/10.1023/A:1005929032764>
- Shangguan, W., Dai, Y., Duan, Q., Liu, B., & Yuan, H. (2014). A global soil data set for earth system modeling. *Journal of Advances in Modeling Earth Systems*, *6*, 249–263. <https://doi.org/10.1002/2013MS000293>
- Song, Y., Cervarich, M., Jain, A. K., Khesghi, H. S., Landuyt, W., & Cai, X. (2016). The interplay between bioenergy grass production and water resources in the United States of America. *Environmental Science & Technology*, *50*(6), 3010–3019. <https://doi.org/10.1021/acs.est.5b05239>
- Song, Y., Jain, A. K., & McIsaac, G. F. (2013). Implementation of dynamic crop growth processes into a land surface model: Evaluation of energy, water and carbon fluxes under corn and soybean rotation. *Biogeosciences*, *10*(12), 8039–8066. <https://doi.org/10.5194/bg-10-8039-2013>
- Song, Y., Jain, A. K., William, L., Khesghi, H. S., & Khanna, M. (2014). Estimates of biomass yield for perennial bioenergy grasses in the USA. *Bioenergy Research*, *8*(2), 688–715. <https://doi.org/10.1007/s12155-014-9546-1>
- Tian, H., Lu, C., Chen, G., Tao, B., Pan, S., Grosso, S. J. D., et al. (2012). Contemporary and projected biogenic fluxes of methane and nitrous oxide in North American terrestrial ecosystems. *Frontiers in Ecology and the Environment*, *10*(10), 528–536. <https://doi.org/10.1890/120057>
- Tian, H., Lu, C., Ciais, P., Michalak, A. M., Canadell, J. G., Saikawa, E., et al. (2016). The terrestrial biosphere as a net source of greenhouse gases to the atmosphere. *Nature*, *531*(7593), 225–228. <https://doi.org/10.1038/nature16946>
- Tian, H., Xu, X., Liu, M., Ren, W., Zhang, C., Chen, G., & Lu, C. (2010). Spatial and temporal patterns of CH₄ and N₂O fluxes in terrestrial ecosystems of North America during 1979–2008: Application of a global biogeochemistry model. *Biogeosciences*, *7*(9), 2673–2694. <https://doi.org/10.5194/bg-7-2673-2010>
- Topp, E., & Pattey, E. (1997). Soils as sources and sinks for atmospheric methane. *Canadian Journal of Soil Science*, *77*(2), 167–177. <https://doi.org/10.4141/S96-107>
- Turetsky, M. R., Kotowska, A., Bubier, J., Dise, N. B., Crill, P., Hornibrook, E. R. C., et al. (2014). A synthesis of methane emissions from 71 northern, temperate, and subtropical wetlands. *Global Change Biology*, *20*(7), 2183–2197. <https://doi.org/10.1111/gcb.12580>
- Wagner, D. (2017). Effect of varying soil water potentials on methanogenesis in aerated marshland soils. *Scientific Reports*, *7*, 14706. <https://doi.org/10.1038/s41598-017-14980-y>
- Walker, A. P., Hanson, P. J., De Kauwe, M. G., Medlyn, B. E., Zaehle, S., Asao, S., et al. (2014). Comprehensive ecosystem model-data synthesis using multiple data sets at two temperate forest free-air CO₂ enrichment experiments: Model performance at ambient CO₂ concentration. *Journal of Geophysical Research: Biogeosciences*, *119*, 937–964. <https://doi.org/10.1002/2013JG002553>
- Wania, R., Ross, I., & Prentice, I. C. (2010). Implementation and evaluation of a new methane model within a dynamic global vegetation model: LPJ-WHyMe v1.3.1. *Geoscientific Model Development*, *3*(2), 565–584. <https://doi.org/10.5194/gmd-3-565-2010>
- Willmott, C. J., Robeson, S. M., & Matsuura, K. (2012). A refined index of model performance. *International Journal of Climatology*, *32*(13), 2088–2094. <https://doi.org/10.1002/joc.2419>
- Xu, X. F., Tian, H. Q., Zhang, C., Liu, M. L., Ren, W., Chen, G. S., et al. (2010). Attribution of spatial and temporal variations in terrestrial methane flux over North America. *Biogeosciences*, *7*(11), 3637–3655. <https://doi.org/10.5194/bg-7-3637-2010>
- Yang, X., Wittig, V., Jain, A. K., & Post, W. M. (2009). Integration of nitrogen dynamics into a global terrestrial ecosystem model. *Global Biogeochemical Cycles*, *23*, GB4028. <https://doi.org/10.1029/2009GB003474>
- Zhang, Z., Zimmermann, N. E., Stenke, A., Li, X., Hodson, E. L., Zhu, G., et al. (2017). Emerging role of wetland methane emissions in driving 21st century climate change. *Proceedings of the National Academy of Sciences*, *114*(36), 9647–9652. <https://doi.org/10.1073/pnas.1618765114>
- Zhao, F., Zeng, N., Ito, A., Asrar, G., Friedlingstein, P., Jain, A. K., et al. (2016). Role of CO₂, climate and land use in regulating the seasonal amplitude increase of carbon fluxes in terrestrial ecosystems: A multimodel analysis. *Biogeosciences*, *13*(17), 5121–5137. <https://doi.org/10.5194/bg-13-5121-2016>
- Zhou, J. L., Tits, A. L., & Lawrence, C. T. (1997). User's guide for FFSQP version 3.7: A Fortran code for solving optimization programs, possibly Minimax, with general inequality constraints and linear equality constraints, generating feasible iterates. (technical report SRC-TR-92-107r5). College Park, MD: Institution for systems research, University of Maryland.
- Zscheischler, J., Michalak, A. M., Schwalm, C. R., Mahecha, M. D., Huntzinger, D. N., Reichstein, M., et al. (2014). Impact of large-scale climate extremes on biospheric carbon fluxes: An intercomparison based on MsTMIP data. *Global Biogeochemical Cycles*, *28*, 585–600. <https://doi.org/10.1002/2014GB004826>